Nanoscale

PAPER

View Article Online
View Journal

Cite this: DOI: 10.1039/c6nr08353f

Amplified impedimetric aptasensor combining target-induced DNA hydrogel formation with pH-stimulated signal amplification for the heparanase assay†

Zhe-Han Yang, Ying Zhuo, Ruo Yuan* and Ya-Qin Chai*

Received 25th October 2016,
Accepted 12th January 2017

DOI: 10.1039/c6nr08353f

rsc.li/nanoscale

Herein, a novel electrochemical impedimetric biosensor for the heparanase (HPA) assay was developed based on target protein-induced DNA hydrogel formation, followed by pH-stimulation of the hydrogel density to increase the signal amplification. The method involved the synthesis of two different copolymer chains, consisting of two cooperatively functioning cross-linking elements, where one element was associated with the HPA-response and the other one with the pH-response. Initially, single-strand DNA as a capture probe was modified on the electrode surface. In the presence of HPA, the HPA-responsive element binding to HPA-induced DNA hybridization between the two copolymer chains and captured DNA, giving rise to the formation of a low-density polymer hydrogel film on the electrode surface and it obtaining an obvious impedimetric response. A significant signal enhancement was observed when changing the pH of the hydrogel film to 5.0, which could be ascribed to the fact that the pH-responsive element can fold into four-stranded i-motif structures at pH 5.0, leading to the increase in density of the hydrogel film. By implementing the DNA hydrogel to induce an impedimetric response change, this impedimetric biosensor exhibited an excellent analytical performance towards the HPA quantitative assay, with a low detection limit of 0.003 pg mL^{-1}. This new method provides a versatile signal amplification method and paves a new way to construct impedimetric sensors for bioassays.

Introduction

Electrochemical impedance spectroscopy (EIS), a label-free electrochemical technique for analyzing electrode-solution interfacial electron transfer, has attracted a great deal of attention in the characterization of materials, corrosion science, fuel cells and batteries.[1] Since EIS has a less destructive effect on the measured biological interactions, a series of efforts has been made to apply EIS in the construction of impedimetric biosensors for the quantification of biomolecular activity.[2] Initially, the impedance changes of impedimetric biosensors only depended on the target's nonconductive property, thus limiting detection sensitivity.[3–6] However, recently, a signal amplification strategy based on enzymatic biocatalytic precipitation has been widely implemented in the construction of impedimetric biosensors, because the precipitation exhibits greater resistance than the target itself for the electron transfer of redox probes.[7,8] However, biomolecular activity, especially enzyme activity, suffers from the influence of the generated precipitation, which causes a poor biocompatibility of these methods.[9–11] Hence, the search for a new method and signal amplification strategy to construct a biocompatible as well as sensitive impedimetric biosensor is still highly desired.

Hydrogels, which comprise 3D network polymers, have received increasing attention in chemistry, biology and medicine for their good biocompatibility, flexibility and mechanical stability.[12–15] Recently, DNA, as an intelligent material, has been used to prepare smart hydrogels, including "all DNA" hydrogel and DNA-modified polymer hydrogel.[16–19] These DNA-based hydrogels can provide the following three outstanding advantages: (1) the hydrogel is biocompatible and sequence programmable;[20,21] (2) the hydrogel can respond to appropriate stimuli, such as pH,[22] light[23] and metal ions,[24,25] by designing the corresponding responsive DNA; (3) hydrogel/solution transitions can be purposely controlled by stimuli-responsive DNA.[26] Therefore, DNA-based hydrogels have begun to be applied in various fields, including controlled drug delivery and release,[27] the activation of biocatalytic cascades,[28] the

Key Laboratory of Luminescent and Real-Time Analytical Chemistry (Southwest University), Ministry of Education, College of Chemistry and Chemical Engineering, Southwest University, Chongqing 400715, PR China. E-mail: yuanruo@swu.edu.cn, yqchai@swu.edu.cn

† Electronic supplementary information (ESI) available: Materials, apparatus and measurements, PAGE analysis, optimized experimental conditions. See DOI: 10.1039/c6nr08353f

controlled release of enzymes,[29] preparation of shape-memory materials[30] and in visual biosensors.[31–33] However, to date, the application of DNA hydrogels in electrochemistry has rarely been reported. Very recently, Gibbs *et al.* assembled a DNA hydrogel containing ferrocene on the surface by a hybridization reaction to electrochemically detect DNA.[34] Willner's group reported a DNA hydrogel with switchable electrocatalytic properties through integration of a K^+ ion/crown ether and a hemin/Gquadruplex assembled on the surface by hybridization chain reaction.[35] Although DNA hydrogels can be assembled on a surface by DNA–DNA hybridization, both the electrocatalytic and electrochemical efficiency is affected by the hydrogel itself and this can greatly hinder electron transfer on surfaces. Specifically, this hindering effect increases with increasing the hydrogel density. On the basis of the above observations, an impedimetric biosensor may be developed by assembling a DNA hydrogel on a surface, and then a signal amplification strategy can be designed by increasing the hydrogel density. To the best of our knowledge, so far, there is no report focusing on using DNA hydrogels for the construction of an amplified impedimetric biosensor.

Heparanase (HPA) is a mammalian *endo*-β-D-glucuronidase that is related to tumour metastasis, development and invasion, thereby presenting as a potential target in cancer therapies.[36] Thus, the monitoring of concertation HPA plays an important role in cancer treatment. In a previous study, various methods, including ELISA and fluorescence assay, were reported for HPA detection.[37,38] To enhance sensitivity, herein, an amplified impedimetric biosensor was developed for monitoring HPA based on target-induced and pH-regulated DNA hydrogel. The principle of our work is illustrated in Schemes 1 and 2. Three acrydite-modified DNA strands were programmed to yield the polymer wire, in which S1 and S2 complement each other with fifteen nucleotides, while S3 including the cytosine-rich sequence can fold and form a bimolecular "i-motif" structure through protonated cytosine–cytosine ($C:C^+$) base-pairing below pH 6.3.[39] Accordingly, the polymer P1 was synthesized by copolymerizing acrylamide monomer units with S1 and S3. Then the S1 fragment in P1 hybridized to HPA aptamer with the formation of a stable S1/aptamer duplex to prepare a recognition polymer. The polymer P2 was synthesized by copolymerizing acrylamide monomer units with S2 and S3. The amino-S4, as a capture probe that is partially complementary to the S1 fragment in the recognition polymer was modified on a Au-coated electrode surface. When only dropping the recognition polymer and P2 onto the modified-electrode surface, S1 could not hybridize to S2 and S4 since both the complementary sequences between S1 and S2, and the complementary sequences between S1 and S4 are shorter than that between S1 and the HPA aptamer. As a result, no hydrogel is formed on the surface of the electrode. However, upon the addition of HPA, S1 can be released from the S1/aptamer duplex by HPA protein–aptamer binding, which triggered the hybridization of S2 and S4 with the S1 fragment, giving rise to the formation of cross-linked polymer hydrogel films on the electrode surface. Therefore, an impedimetric response that is associated with the HPA concentration is read out. Moreover, the impedimetric signal can be further enhanced by increasing the hydrogel density by changing the pH to 5.0, resulting in a high sensitivity of the impedimetric biosensor. This new method paves a new way to construct impedimetric sensors for bioassays.

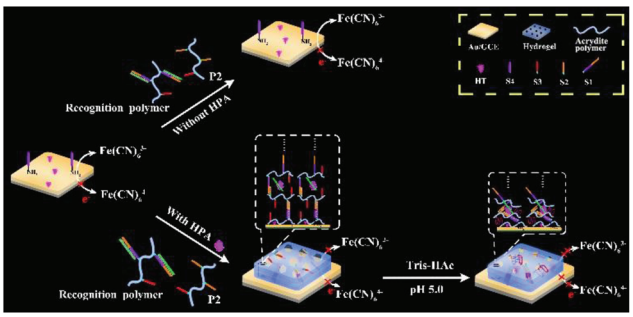

Scheme 2 The HPA-induced DNA hydrogel film formation on Au-coated GCE surface, and pH-stimulation of the hydrogel film density for increased signal amplification.

Results and discussion

UV-visible absorption spectra analysis

As mentioned above, the recognition polymer and P2 were prepared by copolymerizing acrydite–DNA with acrylamide residues. To confirm this process, we used UV-vis absorption spectra to investigate the change in the absorption maximum of the different species. As shown in Fig. 1(A), curve a shows

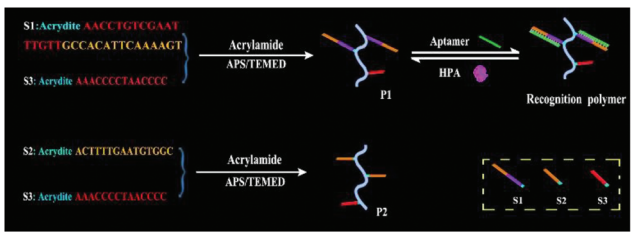

Scheme 1 Synthesis of the acrylamide–acrydite–DNA polymer P1, P2 and a recognition polymer.

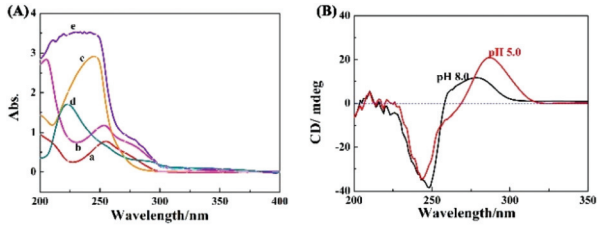

Fig. 1 (A) UV-vis absorption spectrum of: DNA (a), acrydite–DNA (b), acrydite monomer (c), acrydite polymer (d) and DNA-modified acrydite polymer (e). (B) CD spectra corresponding to: the acrylamide hydrogel structure at pH 8.0 (black line) and at pH 5.0 (red line).

the UV-vis absorption spectrum of DNA, and here, a distinct spectral profile with an absorption maximum at 260 nm was observed. However, the absorption position of the same DNA sequence with the acrydite shifted slightly towards shorter wavelength regions is seen with curve b, with the absorption maximum wavelength at 251 nm. This result might be caused by introducing an acrydite group. Curve c shows the absorption spectrum of the acrydite monomer, it can be seen that the absorption maximum wavelength is at 245 nm. Once the acrydite monomer is copolymerized, the absorption maximum wavelength is achieved at 223 nm (curve d). The absorption position was shifted towards shorter wavelength regions in comparison with acrydite monomer due to the π-conjugated system disappearing in the polymer. When acrydite–DNA was copolymerized with acrylamide monomers, a wide absorption band could be observed (curve e). The reason for this might be most likely a consequence of the fact that both the DNA and acrydite polymer simultaneously exist in the DNA-modified polymer and both absorb the visible light.

Circular dichroism spectroscopy analysis

The hydrogel formed at pH 8.0 by duplex nucleic acid bridges and the pH-induced formation of four-stranded i-motif units at pH 5.0 were supported by circular dichroism (CD) measurements, as seen in Fig. 1B. The CD spectrum of the hydrogel at pH 8.0 is depicted by curve a, where it can be seen that the hydrogel shows a positive band at 268 nm, which represents a standard duplex CD spectrum.[40] Subjecting the pH of the hydrogel to 5.0 results in a positive band at 288 nm (curve b), which is consistent with the reported spectrum of a four-stranded i-motif structure,[41] indicating the formation of four-stranded i-motif structures at pH 5.0. These results gave additional evidence that the density increase of the hydrogel was indeed induced by the motion of the i-motif DNA motors, as designed.

Characterizations of the hydrogel on the surface

The 3D network structure of the hydrogel and the pH-induced pore size transition were investigated by using SEM. In the hydrogel system of the cross-linked polymer backbones, the resulting pores provide the host environment for the water nanodroplets. A porous network structure would be obtained after freezing these water nanodroplets and subliming them under vacuum. As shown in Fig. 2A, the freeze-dried hydrogel revealed very large pores surrounded by the polymer, and a network structure can be obviously observed. Interestingly, the insert image shows that the network backbone also exhibits a pore structure. After changing the pH of the hydrogel film to 5.0 by incubating tris-HAc (pH 5.0, Fig. 2B), a denser structure of 3D network and a smaller diameter of pore could be observed, indicating that the pH could indeed induce a pore size transition, because the S3 i-motif yields a high degree cross-linking polymer network system.

To show the fine structural changes in the hydrogel backbone under different pH values, AFM measurements were conducted. Fig. 2C shows an AFM image of the HT/S4/Au-modified surface, where the surface tends to show a granular morphology. When the 3D network hydrogel film is formed on the HT/S4/Au surface, the granular morphology disappears (Fig. 2D). More importantly, a hydrogel backbone with a high porosity and large pore diameter also can be clearly observed. After the hydrogel film is immersed in the tris-HAc buffer (pH 5.0) for 2 h, a hydrogel film backbone with a narrow pore diameter is formed, as shown in Fig. 2E.

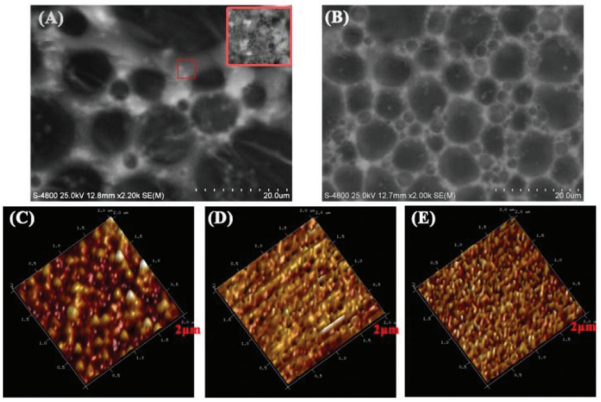

Fig. 2 Freeze-dried SEM images corresponding to: (A) the hydrogel formed on the surface at pH 8.0, and (B) the dense structure generated at pH 5.0. AFM images are present to show the detailed hydrogel backbone structure corresponding to: (C) the HT/S4/AuNPs modified surface, (D) the hydrogel formed on the surface at pH 8.0, and (E) a denser structure generated at pH 5.0.

Studies of the modified GCE

The aptasensor surface at each fabrication step was characterized by EIS in 2.5 mM of $[Fe(CN)_6]^{3-/4-}$. Nyquist plots show a semicircle, in which the straight line corresponds to the Warburg-impedance (Z_w) and the diameter corresponds to the charge-transfer resistance (R_{ct}). The experimental results are shown in Fig. 3. Here, compared with the bare GCE (curve a),

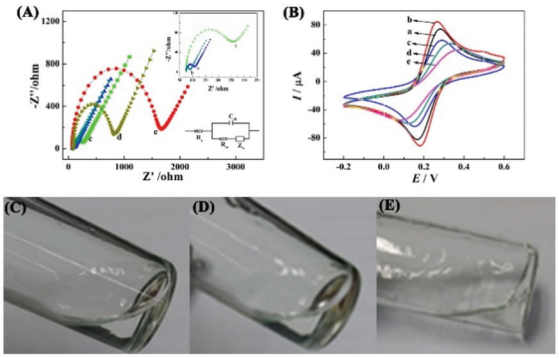

Fig. 3 EIS (A) and CV (B) of different modified electrodes in PBS buffer containing 2.5 mM $[Fe(CN)_6]^{3-/4-}$: (a) bare GCE; (b) Au/GCE; (c) S4/Au/GCE; (d) HT/S4/Au/GCE; (e) hydrogel/HT/S4/Au/GCE. Photograph of the mixture of P2 and the recognition polymer at pH 8.0 (C), the mixture of P2, the recognition polymer and HPA at pH 8.0 (D), the mixture of P2, the recognition polymer and HPA at pH 5.0 (E).

the R_{ct} value of the AuNP-layer-modified GCE (curve b) is remarkably decreased. This result can be ascribed to the AuNP layer not only contributing to the increase in the charge-transfer rate but also enhances the electrode effective area. After the amino-modified S4 was connected to AuNP, the R_{ct} value is increased because of the additional negative charge from the nucleic acid strand (curve c). Once HT as a blocking agent was incubated on the modified electrode, a further increase in R_{ct} was observed (curve d). When P2, the recognition polymer and HPA were incubated, the R_{ct} value was increased greatly, indicating that the target HPA successfully induced the formation of the hydrogel on the modified-electrode surface (curve e). CV was also used to further provide information about the preparation of the aptasensor. The results are presented in Fig. 3B. It can be seen that the information provided by the current changes agreed with that of the R_{ct} value change, indicating that the aptasensor was successfully constructed.

In addition, Fig. 3C shows a photograph of the mixture of P2 and the recognition polymer, in which a liquid phase can be observed. When introducing HPA into the mixture solution, phase translation could not observed with the naked eye, indicating that HPA recognition could only induce low-density hydrogel formation, which was not enough to trigger an obvious phase translation (Fig. 3D). After changing the pH to 5.0, a hydrogel with a high density could be observed, suggesting that the pH could indeed stimulate the density of the hydrogel to increase (Fig. 3E).

pH-Stimulated density increase of the hydrogel for signal amplification

S3 contained in the hydrogel film can fold and form a bimolecular four-stranded i-motif structure below pH 6.3, resulting in a more stable and denser hydrogel film on the surface for amplifying the EIS signal. First, the pH value of the tris-HAc buffer and the incubation time were optimized to obtain the maximum value of EIS intensity signal, as shown in Fig. S3.† Then, a comparison of the EIS response before and after changing the pH of the hydrogel film to 5.0 was investigated. As shown in Fig. 4A, curve a revealed the EIS response when HPA induced the formation of the hydrogel film on the electrode surface. After changing the pH of the hydrogel film to 5.0, the R_{ct} value was increased by 168% (curve b). These results indicate that the pH-stimulated formation of i-motif structures of S3 indeed enhanced the hindrance of electron transfer and amplified the EIS signal.

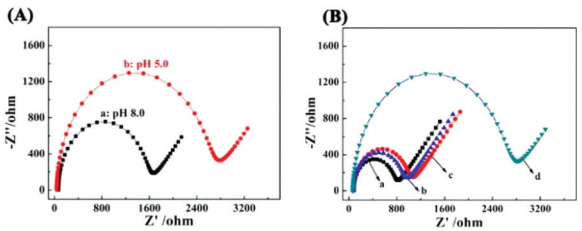

Fig. 4 (A) EIS response in PBS buffer (pH 7.0) containing 2.5 mM $[Fe(CN)_6]^{3-/4-}$ when the hydrogel film is formed on the modified-electrode surface at pH 8.0 (curve a) and after changing the pH of the hydrogel film to 5.0 (curve b). (B) Comparison of the EIS responses of different modified electrodes: (a) HT/**S4**/Au/GCE; (b) recognition polymer, P2, **HPA**/HT/Au/GCE; (c) recognition polymer, P2/TH/**S4**/Au/GCE; (d) recognition polymer, P2, **HPA**/HT/**S4**/Au/GCE.

Estimation of the effect of S4 and HPA protein on the formation of the hydrogel film

Because physical adhesion of the hydrogel on the surface was unstable in this system, S4 as a capture DNA was immobilized on the electrode surface to stabilize the hydrogel on the electrode surface by forming an S4/S1 duplex. To verify this issue, a control experiment was designed, where the electrode modification process was the same as the proposed aptasensor except for no S4 immobilization. As shown in Fig. 4B, the EIS value of the control experiment (curve b) was close to that of HT/S4/Au/GCE (curve a), but significantly less than the EIS value of the proposed aptasensor (curve d). The reason for this might be ascribed to the fact that a hydrogel film was not formed on the electrode surface when no S4 is immobilized, demonstrating that S4 played a vital role in the formation of the hydrogel film on the surface of the electrode. In addition, to investigate the effect of the aptamer–HPA protein recognition on formation of the hydrogel film, a blank experiment was conducted. Curve c shows the experimental result of this, and it can be seen that the EIS response was also close to that of HT/S4/Au/GCE, but greatly less than the proposed aptasensor. This result confirmed the fact that the aptamer–HPA protein recognition induced the formation of the hydrogel film on the electrode surface.

CVs behaviour at different scan rates

CVs at different scan rates were conducted to further investigate the electron transfer process in the hydrogel-film-modified electrode. As can be seen from Fig. 5A, the redox peak current and potential gap increased with increasing the scan rates. Furthermore, both the anodic and cathodic peak currents were proportional to the square root of scan rate ($v^{1/2}$) in the range of 10–300 mV s^{-1} and showed a good linear relationship (Fig. 5B). The results demonstrate that the whole electrochemical process of the hydrogel-film-modified electrode was controlled by diffusion. The electrochemical behaviour was consistent with a 3D-nanoporous-material-modified electrode reported in previous studies.[40]

Performance of the aptasensor

To test the sensitivity of the aptasensor, a series of HPAs with various concentrations were determined. As shown in Fig. 5C, an increase in the relative EIS value with a higher concentration of target HPA was observed. This was attributed to the fact that a higher concentration of target HPA causes a larger amount of hydrogel to be formed on the electrode surface, resulting in a higher EIS signal response. In addition, the detection sensitivities were determined to be 0.3 pg mL^{-1} with a linear range of 0.001 ng mL^{-1}–10 ng mL^{-1} and

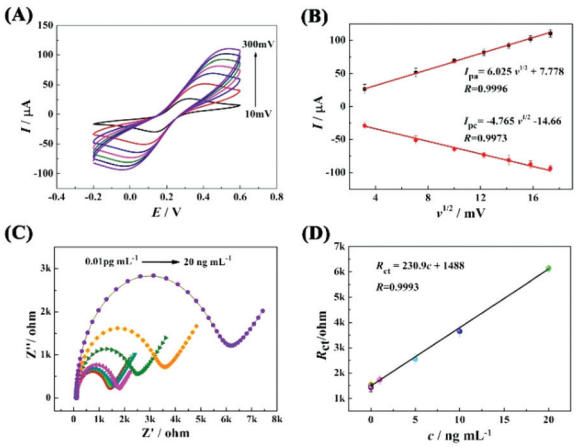

Fig. 5 (A) CV response in PBS buffer containing 2.5 mM $[Fe(CN)_6]^{3-/4-}$ at different scan rates: 10, 50, 100, 150, 200, 250 and 300 mV s^{-1}. (B) Plots of the redox peak currents *vs.* the different scan rates. (C) EIS responses of the proposed aptasensor after incubation with different concentrations of HPA. (D) Signal responses of the aptasensor to the concentration of HPA.

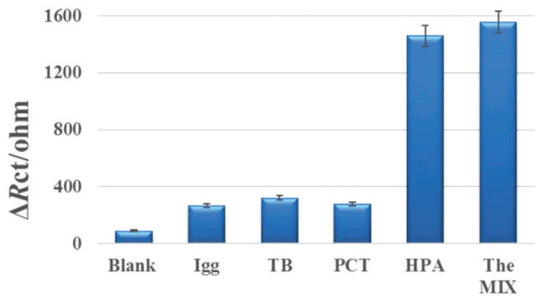

Fig. 6 The specificity of the impedimetric aptasensor.

0.003 pg mL^{-1} with a linear range of 0.01 pg mL^{-1} to 20 ng mL^{-1} before and after pH-stimulation, respectively. The sensitivity improvement was achieved owing to S3 self-assembling at pH 5.0 into an i-motif structure, also increasing the density of hydrogel films. This results in an amplified EIS response after incubation of the same concentration of target HPA as compared to a biosensor without pH-stimulation. Furthermore, both the detection limit and linear range are superior or comparable with those of existing protein electrochemical assays described in the literature (Table 1).

To evaluate the aptasensor in our assay for the selectively targeted HPA, three unrelated proteins, including thrombin (TB), haemoglobin (IGg) and procalcitonin (PCT), were assessed by comparing the EIS signals of the modified electrode incubated with the three proteins to that of the target HPA under the same experimental conditions (Fig. 6). An excessive unrelated proteins concentration of 100 nM was used to test the aptasensor specificity. It was found that the EIS signals from the experiments involving IGg, TB and PCT were similar to the blank control. In contrast, the EIS signal from the detection of HPA was about 10-fold higher than the signals of these unrelated proteins. These experimental results indicate the high specificity of our aptasensor for target HPA recognition and for subsequent electrochemical detection.

To evaluate the stability of the proposed biosensor, a long-term stability experiment was also performed *via* storing the biosensor at 4 °C and assaying every 4 days. Five of the aptasensors with 1.0 ng mL^{-1} HPA were determined under the same experimental conditions. After 20 days, the EIS responses retained 91.2%, 93.3%, 94.7%, 90.1% and 94.9% of their initial EIS values, indicating that the aptasensor had good stability. The results demonstrate that the hydrogel film could be stabilized on an electrode surface by using a DNA duplex to immobilize the hydrogel film.

Clinical serum samples analysis

After establishing the detection sensitivity and specificity towards the target HPA, we then challenged the assay in human serum sample to investigate aptasensor performance with more complex biological samples. First, 1 mL healthy human serum samples were diluted with 0.1 M PBS (pH 7.0) to reach a final volume of 10 mL. Then, the obtained human serum sample was used to dilute a serious of concentrations of standard HPA samples. After that, the prepared aptasensor was incubated with the above HPA samples to assess the influence of the serum samples for the HPA assay. Table 2 shows the experimental results, where it can be seen that the recovery varied from 90.2% to 110% and the RSDs ranged from 7.36% to 9.35%. These results clearly suggest that our proposed aptasensor could be applied for the HPA assay in complex biological samples.

Table 1 Comparison of the proposed aptasensor with other reported impedimetric biosensors

Sensor type	Detection limit (ng mL^{-1})	Detection range (ng mL^{-1})	Ref.
EIS signal change induced by target itself	0.006	0.004–40.3	41
EIS signal change induced by target itself	0.08	0.17–16.5	42
EIS signal change induced by target itself	0.002	0.01–10	43
EIS signal change induced by enzymatic biocatalytic precipitation	0.05	0.01–30	44
EIS signal change induced by enzymatic biocatalytic precipitation	3.8×10^{-4}	5.0×10^{-4}–40	45
EIS signal change induced by DNA hydrogel	3.0×10^{-6}	1.0×10^{-5}–20	This work

Table 2 Recovery results of the proposed aptasensor in human serum

Sample no.	Added (ng mL^{-1})	Found (ng mL^{-1})	Recovery (%)	RSD (%)
1	0.010	0.00996	99.6	9.35
2	0.10	0.095	95	7.36
3	1.0	1.10	110	8.99
4	5.0	4.51	90.2	9.16

Conclusion

In summary, the present study developed a novel amplified impedimetric aptasensor by generating DNA hydrogel films on an electrode surface. Through target HPA-induced DNA hydrogel formation on the electrode surface, an obvious impedimetric response could be obtained for the inherent nonconductive property of the hydrogel. Simultaneously, the impedimetric signal could be further enhanced by changing the pH value to increase the density of the pH-responsive hydrogel, which significantly improved the analytical sensitivity of the impedimetric biosensor. Additionally, with the introduction of the hydrogel into an impedimetric biosensor, the biocompatibility was improved. Moreover, this method can potentially be further extended to the portable quantitative detection of various targets, including metal ions, protein, DNA and microRNA, by replacing the target-responsive DNA. In view of these advantages, such systems may create a new method to construct impedimetric biosensors.

Experimental

Live subject statement

All the studies involving live subjects were carried out under the guidance of the Experiment Management Committee of Southwest University and approved by the Institutional Ethical Committee. All the experiments were performed in compliance with the relevant laws and institutional guidelines.

Synthesis of the acrylamide copolymer chain

Acrydite-modified DNA was used to synthesize the copolymer chains.[35] As shown in Scheme 1, the recognition polymer was prepared by adding 60 μL of S1 (100 μM), 80 μL of S3 (100 μM), 80 μL of aptamer (100 μM) and 25 μL of acrylamide (40%) into 175 μL of buffer solution (Tris-HCl, 10×10^{-3} M, pH 8.0). P2 was prepared by adding 60 μL of S2 (100 μM), 80 μL of S3 (100 μM) and 25 μL of acrylamide (40%) into 235 μL of buffer solution (Tris-HCl, 10×10^{-3} M, pH 8.0). Then, nitrogen was bubbled through the above two solutions for 3 min, respectively. Subsequently, 4 μL of the initiator (100 μL initiator solution containing 10 mg APS and 5 μL TEMED) was added to the two prepared solutions, respectively. The two samples were allowed to polymerize at room temperature for 5 min and were then incubated at 4 °C for a time interval of 12 h to form the copolymer chains. Finally, the resulting polymers' recognition polymers and P2 were filtered through a MWCO 30 kDa column to eliminate unpolymerized strands monomer units, salts and initiator, and the resultant solution was then stored at 4 °C for further use.

Electrochemical impedimetric detection of HPA

First, GCE with a mirror-like surface was obtained by polishing it with 0.3 and 0.05 μm alumina powder. After that, the GCE was sonicated in ultrapure water and rinsed thoroughly. The AuNP-layer-modified GCE was obtained by soaking the clean GCE in $HAuCl_4$ solution (1%, w/w) and electrodepositing at −0.2 V for 30 s. Then, NH_2-terminated S4 (10 μL, 2.5 μM) was immobilized on the electrode surface by Au–N bonds after incubation for 16 h at room temperature. To block the remaining active sites, HT solution (10 μL, 1%, w/w) was incubated on the surface of the modified electrode for 40 min. Subsequently, the recognition polymer (6.7 μL), P2 (6.7 μL) solution and HPA (6.7 μL) standard solution with different concentrations were dropped onto the resulting electrode surface and incubated for 2 h at room temperature. To remove the physically adsorbed species, the modified electrode was thoroughly cleaned with ultrapure water. Finally, a tris-HAc buffer solution that included sodium chloride (0.5 M) and magnesium chloride (0.1 M), pH 5.0 was dropped onto the electrode surface and reacted for 2 h. The electrochemical signal was carried out in 2.5 mM $[Fe(CN)_6]^{3-/4-}$ (pH 7.0), which gave the quantitative criteria for the electrochemical detection of HPA.

Electrochemical measurements

EIS was conducted over a frequency range from 10 kHz to 0.1 Hz using an alternative voltage with an amplitude of 5 mV superimposed on a dc potential of 0.22 V. The obtained EIS spectra were fitted by using ZSimpWin electrochemical impedance modelling software to a modified Randles equivalent circuit. The CV experiments were conducted at a scan rate of 100 mV s^{-1}. Both the EIS and CV measurements were recorded in 0.01 M PBS buffer solution containing 2.5 mM $[Fe(CN)_6]^{3-/4-}$ redox pair (1 : 1 molar ratio).

Acknowledgements

The authors are grateful for the National Natural Science Foundation of China (21575116, 51473136), the Fundamental Research Funds for the Central Universities (XDJK2015A002), China.

References

1 X. Dominguez-Benetton, S. Sevda, K. Vanbroekhoven and D. Panta, *Chem. Soc. Rev.*, 2012, **41**, 7228–7246.
2 A. Bonanni, A. H. Loo and M. Pumera, *Trends Anal. Chem.*, 2012, **37**, 12–21.

3 E. Amit, R. Obena, Y.-T. Wang, R. Zhuravel, A. J. F. Reyes, S. Elbaz, D. Rotem, D. Porath, A. Friedler, Y. J. Chen and S. Yitzchaik, *Chem. Sci.*, 2015, **6**, 4756–4766.
4 T. Bryan, X. Luo, L. Forsgren, L. A. Morozova-Roched and J. J. Davis, *Chem. Sci.*, 2012, **3**, 3468–3473.
5 L. Han, P. Liu, V. A. Petrenko and A. Liu, *Sci. Rep.*, 2016, **6**, 22199–22209.
6 M. Labib, A. S. Zamay, O. S. Kolovskaya, I. T. Reshetneva, G. S. Zamay, R. J. Kibbee, S. A. Sattar, T. N. Zamay and M. V. Berezovski, *Anal. Chem.*, 2012, **84**, 8966–8969.
7 J. Zhuang, W. Lai, M. Xu, Q. Zhou and D. Tang, *ACS Appl. Mater. Interfaces*, 2015, **7**, 8330–8338.
8 R. Akter, M. A. Rahman and C. K. Rhee, *Anal. Chem.*, 2012, **84**, 6407–6415.
9 R. M. Kong, T. Fu, N. N. Sun, F. L. Qu, S. F. Zhang and X. B. Zhang, *Biosens. Bioelectron.*, 2013, **50**, 351–355.
10 K. Feng, R. M. Kong, H. Wang, S. F. Zhang and F. L. Qu, *Biosens. Bioelectron.*, 2012, **38**, 121–125.
11 Y. Zhao, Y. Zheng, R. M. Kong, L. Xia and F. L. Qu, *Biosens. Bioelectron.*, 2016, **75**, 383–388.
12 L. Peng, C. Sam Wu, M. You, D. Han, Y. Chen, T. Fu, M. Ye and W. Tan, *Chem. Sci.*, 2013, **4**, 1928–1938.
13 D. J. Beebe, J. S. Moore, J. M. Bauer, Q. Yu, R. H. Liu, C. Devadoss and B. H. Jo, *Nature*, 2000, **404**, 588–590.
14 C. H. Lu, X. J. Qi, R. Orbach, H. H. Yang, I. Mironi-Harpaz, D. Seliktar and I. Willner, *Nano Lett.*, 2013, **13**, 1298–1302.
15 F. L. Qu, Y. Zhang, A. Rasooly and M. H. Yang, *Anal. Chem.*, 2014, **86**, 973–976.
16 T. Liedl, H. Dietz, B. Yurke and F. Simmel, *Small*, 2007, **3**, 1688–1693.
17 H. Meng and G. Li, *Polymer*, 2013, **54**, 2199–2221.
18 K. K. Julich-Gruner, C. Löwenberg, A. T. Neffe, M. Behl and A. Lendlein, *Chem. Phys.*, 2013, **214**, 527.
19 E. Cheng, Y. Xing, P. Chen, Y. Yang, Y. Sun, D. Zhou, L. Xu, Q. Fan and D. S. Liu, *Angew. Chem., Int. Ed.*, 2009, **48**, 7660–7663.
20 F. Liu and M. W. Urban, *Prog. Polym. Sci.*, 2010, **35**, 3–23.
21 M. A. C. Stuart, W. T. S. Huck, J. Genzer, M. Muller, C. Ober, M. Stamm, G. B. Sukhorukov, I. Szleifer, V. V. Tsukruk, M. Urban, F. Winnik, S. Zauscher, I. Luzinov and S. Minko, *Nat. Mater.*, 2010, **9**, 101–113.
22 W. Guo, C. H. Lu, X. J. Qi, R. Orbach, M. Fadeev, H. H. Yang and I. Willner, *Angew. Chem., Int. Ed.*, 2014, **53**, 10134–10138.
23 Y. Yang, M. Endo, K. Hidaka and H. Sugiyama, *J. Am. Chem. Soc.*, 2012, **134**, 20645–20653.
24 Y. Huang, Y. Ma, Y. Chen, X. Wu, L. Fang, Z. Zhu and C. J. Yang, *Anal. Chem.*, 2014, **86**, 11434–11439.
25 H. Lin, Y. Zou, Y. Huang, J. Chen, W. Y. Zhang, Z. Zhuang, G. Jenkins and C. J. Yang, *Chem. Commun.*, 2011, **47**, 9312–9314.
26 T. Zhou, P. Chen, L. Niu, J. Jin, D. Liang, Z. Li, Z. Yang and D. Liu, *Angew. Chem., Int. Ed.*, 2012, **51**, 11271–11274.
27 A. S. Hoffman, *J. Controlled Release*, 2008, **132**, 153–163.
28 S. Lilienthal, Z. Shpilt, F. Wang, R. Orbach and I. Willner, *ACS Appl. Mater. Interfaces*, 2015, **7**, 8923–8931.
29 Z. Zhu, C. Wu, H. Liu, Y. Zou, X. Zhang, H. Kang, C. J. Yang and W. Tan, *Angew. Chem., Int. Ed.*, 2010, **49**, 1052–1056.
30 C. H. Lu, W. Guo, Y. Hu, X. J. Qi and I. Willner, *J. Am. Chem. Soc.*, 2015, **137**, 15723–15731.
31 L. Yan, Z. Zhu, Y. Zou, Y. Huang, D. Liu, S. Jia, D. Xu, M. Wu, Y. Zhou, S. Zhou and C. J. Yang, *J. Am. Chem. Soc.*, 2013, **135**, 3748–3751.
32 H. Yang, H. Liu, H. Kang and W. Tan, *J. Am. Chem. Soc.*, 2008, **130**, 6320–6321.
33 A. Baeissa, N. Dave, B. D. Smith and J. Liu, *ACS Appl. Mater. Interfaces*, 2010, **2**, 3594–3600.
34 J. M. Gibbs, S. J. Park, D. R. Anderson, K. J. Watson, C. A. Mirkin and S. B. T. Nguyen, *J. Am. Chem. Soc.*, 2005, **127**, 1170–1178.
35 J. S. Kahn, A. Trifonov, A. Cecconello, W. Guo, C. Fan and I. Willner, *Nano Lett.*, 2015, **15**, 7773–7778.
36 Y. Y. Wang, R. Zhou, B. Zhou, T. Wang, L. Zhang and D. Luo, *Int. J. Clin. Exp. Med.*, 2015, **8**, 18107–18114.
37 W. Zhang, H. C. Yang, Q. Wang, Z. J. Yang, H. Chen, S. M. Wang, Z. M. Pan, B. J. Tang, Q. Q. Li and L. Li, *Anticancer Res.*, 2011, **31**, 3423–3428.
38 C. M. o. Melo, I. L. S. Tersariol, H. B. Nader, M. A. S. Pinhal and M. A. Lima, *Catal. Rev.*, 2015, **412**, 66–70.
39 Z. Zhao, L. Wang, Y. Liu, Z. Yang, Y. M. He, Z. Li, Q. H. Fan and D. S. Liu, *Chem. Commun.*, 2012, **48**, 9753–9755.
40 Y. Sun, H. Liu, L. Xu, L. Wang, Q. H. Fan and D. S. Liu, *Langmuir*, 2010, **26**, 12496–12499.
41 L. Rivas, C. C. Mayorga-Martinez, D. Quesada-Gonzalez, A. Zamora-Galvez, A. Escosura-Muñiz and A. Merkoci, *Anal. Chem.*, 2015, **87**, 5167–5172.
42 R. Elshafey, M. Siaj and M. Zourob, *Biosens. Bioelectron.*, 2015, **68**, 295–302.
43 H. Jo, S. K. Kim, H. Youn, H. Lee, K. Lee, J. Jeong, J. Mok, S. H. Kim, H. S. Park and C. Ban, *Biosens. Bioelectron.*, 2016, **81**, 80–86.
44 L. L. Ding, J. P. Ge, W. Q. Zhou, J. P. Gao, Z. Y. Zhang and Y. Xiong, *Biosens. Bioelectron.*, 2016, **85**, 212–219.
45 L. Hou, Y. Tang, M. Xu, Z. Gao and D. Tang, *Anal. Chem.*, 2014, **86**, 8352–8358.